Role of bases in quantum optimal control

The Role of Bases in Quantum Optimal Control

Alice Pagano,[1,2,3] Matthias M Müller,[4] Tommaso Calarco,[4,5,6] Simone Montangero,[1,2,3] and Phila Rembold[2,5,7]

[1]*Institute for Complex Quantum Systems, Ulm University, Albert-Einstein-Allee 11, 89069 Ulm, Germany*
[2]*Dipartimento di Fisica e Astronomia "G. Galilei" & Padua Quantum Technologies Research Center, Università degli Studi di Padova, 35131 Padova, Italy*
[3]*INFN, Sezione di Padova, via Marzolo 8, 35131 Padova, Italy*
[4]*Peter Grünberg Institute – Quantum Control (PGI-8), Forschungszentrum Jülich GmbH, 52425 Jülich, Germany*
[5]*Institute for Theoretical Physics, University of Cologne, 50937 Köln, Germany*
[6]*Dipartimento di Fisica e Astronomia, Università di Bologna, 40127 Bologna, Italy*
[7]*Atominstitut, Technische Universität Wien, Stadionallee 2, 1020 Wien, Austria*

(Dated: August 7, 2024)

Quantum Optimal Control (QOC) supports the advance of quantum technologies by tackling its problems at the pulse level: Numerical approaches iteratively work towards a given target by parametrising the applied time-dependent fields with a finite set of variables. The effectiveness of the resulting optimisation depends on the complexity of the problem and the number of variables. We consider different parametrisations in terms of basis functions, asking whether the choice of the applied basis affects the quality of the optimisation. Furthermore, we consider strategies to choose the most suitable basis. For the comparison, we test three different randomisable bases – introducing the sinc and sigmoid bases as alternatives to the Fourier basis – on QOC problems of varying complexity. For each problem, the basis-specific convergence rates result in a unique ranking. Especially for expensive evaluations, e.g., in closed-loop, a potential speed-up by a factor of up to 10 may be crucial for the optimisation's feasibility. We conclude that a problem-dependent basis choice is an influential factor for QOC efficiency and provide advice for its approach.

I. INTRODUCTION

Quantum optimal control theory resulted in the development of a family of algorithms that iteratively adjust time-dependent control fields to improve a given quantum process [1–5]. The quality of said process is quantified by a figure of merit (FoM) which is minimised (or maximised). When the full classical description of the quantum system is available, the most cost-efficient way to optimise them is typically via a numerical simulation of this model, or in other words with an open-loop approach [6, 7]. However, when the system is expensive to characterise in its entirety – including transfer functions, noise, environmental factors, etc. – a closed-loop approach [8–14] is more effective. This type of optimisation relies on a direct connection between the experiment and the algorithm. In most optimisation algorithms the control pulses are expanded in terms of basis functions. Certain methods such as (d)CRAB [15, 16] or GOAT [17] typically use smooth basis functions, such as the (random) Fourier basis. Other methods like GRAPE or Krotov split the pulse into piecewise constant segments [18]. In the context of this work we interpret them as elements of a fixed-width square-pulse basis. While the basis does not have to be orthogonal, it must cover a suitable area of the accessible function space in order not to impose a too tight constraint. Many bases meet these criteria. For open-loop optimisations, where the gradients of the FoM are available, the piecewise-constant basis [19] is very popular as it mirrors the most common modelling techniques for quantum dynamics [20]. The information provided by an accessible gradient allows gradient-based techniques to efficiently explore large candidate spaces. However, it has been shown that even for gradient-based methods employing other bases may increase accuracy, flexibility, efficiency, and smoothness [17, 21, 22]. The introduction of a truncated basis can also be studied from an information-theoretical perspective by comparing the information content of the control to the number of degrees of freedom required by the FoM (dimensionality of the problem). From such considerations it follows that the truncated basis has to be large enough to match the dimensionality of the problem [23–25]. Nevertheless, the basis is often chosen according to the default associated with a given QOC algorithm with the common attitude that any large enough set should equivalently be able to find the same solutions. Below, we show how such an attitude can adversely affect the efficiency of the optimisation.

Motivation – Two main arguments support the careful consideration of the basis: First, the number of basis elements required to reconstruct a known solution clearly depends on the chosen basis: It is simple to assemble a fast oscillating pulse with Fourier elements but complex with the piecewise-constant basis. For some problems, all local solutions share certain traits. As a result, bases that can reproduce the relevant pulse properties will be more likely to converge to a good local optimum. Examples are provided in Ref. [26, 27], where the authors show that the found solutions always consist of linear and bang-bang segments, which require high complexity when decomposed via the Fourier basis. A further illustration of the significance of a problem-tailored basis is provided in the context of noise characterisation [28], where it determines how well the system properties can be reconstructed. Second, within a basis, each element has a distinct impact on the system. Considering a non-contributing basis element whose adaption results in no change of the FoM, will result in a slower convergence. This could, e.g., be the case for a frequency component that exceeds the time scale of the system or, in some cases, a basis element that does not change the integral of the pulse. Lastly, a basis may be chosen deliberately to encode control limitations such as limited rise times

or bandwidth restrictions [13, 17].

Approach – To systematically explore the impact of the basis choice on the convergence of the optimisation, we consider two well-explored QOC problems: The state transfer in an Ising chain controlling only the coupling between spins [16], and the optimisation of a qubit NOT gate in the presence of a third, slightly detuned energy level [29]. For each example, we compare three bases chosen for their distinct properties. The optimisations are executed using the dCRAB (dressed Chopped RAndom Basis [5, 16]) formalism in a gradient-free setting to show their applicability in situations with limited access to information about the system and some are reproduced using automatic differentiation [30]. The majority of optimisations was implemented using the QuOCS software suite [31]. We find that the convergence rate of the optimisation is highly dependent on the employed basis and that their ranking differs for each problem. The reasons for that become clearer when analysing the average solutions. We conclude that a problem-dependent basis choice is an influential factor for QOC efficiency. Hopefully, our results will lead to more efficient applications of QOC in the future.

Outline – Sec. II starts with a description of the different bases. In Sec. III we examine two distinct physical models and assess how the choice of basis affects the associated optimisation tasks. From those examples we formulate some advice for picking a basis in Sec. IV. Lastly, the results are summarised in Sec. V, where we give an outlook.

II. BASES

In this work, pulses are constructed according to the dCRAB formalism [5]. Here, a given number N_s of basis vectors is optimised at a time. This process is referred to as a superiteration. After it converges, a new basis vector is constructed from randomly assembled basis elements each characterised by a superparameter s. This basis vector is added to the previously converged solution $c_{\text{fin}}^{J-1}(t)$ and optimised in the next superiteration. Each basis element $f(s, \vec{A}; t)$ is defined by the corresponding optimisation parameter(s) $\vec{A}$. The full pulse $c_i^J(t)$ at iteration i within the J^{th} superiteration is written as

$$\begin{aligned} c_i^J(t) &= c_{\text{fin}}^{J-1}(t) + u_i^J(t) \\ &= \sum_{j=1}^{J-1} u_{\text{fin}}^j(t) + u_i^J(t), \end{aligned} \tag{1}$$

where $u_i^J(t)$ is the pulse optimised in each superiteration with N_s superparameters, given by:

$$u_i^J(t) = \sum_{n=1}^{N_s} f(s_n^J, \vec{A}_i; t) \left[+ f_0(A_{0i}; t) \right]. \tag{2}$$

The last term f_0 refers to a special basis element that is optimised in every superiteration, which is only relevant for the basis in Sec. II C.

The following bases have been chosen as they fit in the dCRAB framework and represent a diverse set of properties. For that reason the popular piece-wise constant basis was replaced by the sigmoid basis in this work [32].

A. Fourier

The Fourier basis [15] is composed of frequency elements. The randomised superparameter corresponds to the frequency s. For each superparameter, there are two optimisation parameters $A = [A^1, A^2]$. Thus, the number of optimisation parameters is $N_{\text{opt}} = 2N_s$ and a basis element can be written as:

$$f(s, [A^1, A^2]; t) = A^1 \sin(st) + A^2 \cos(st). \tag{3}$$

Frequency limits are implemented via a corresponding bandwidth window $0 < s \leq \omega_{\max}$ to choose the superparameters from. The superparameters are picked at random from equally distributed bins in the frequency range (see Ref. [4] for a detailed explanation). An example of pulse constructed by Fourier elements is depicted in Fig. 1.

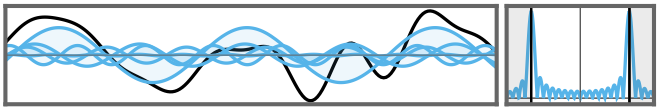

Figure 1: Fourier basis. Left: An example pulse (black) decomposed with Fourier elements (blue). Right: Spectrum of a basis element with $s = \omega_{\max}$ indicated by vertical lines. The cut-off at the start and end time of the pulse leads to the spillage to higher frequencies.

B. Sinc

The sinc basis is composed of wave packets with a fixed bandwidth $\omega_{\max}$. The randomised superparameter corresponds to the center time of the wave packet. The amplitude A of each wave packet is optimised. The basis element f is:

$$f(s, A; t) = A\text{sinc}(\omega_{\max}(t - s)). \tag{4}$$

The number of optimisation parameters is $N_{\text{opt}} = N_s$ and the frequency is limited by $\omega_{\max}$ as the spectrum of a sinc function is a top-hat function of width $\omega_{\max}$, as shown in Fig. 2.

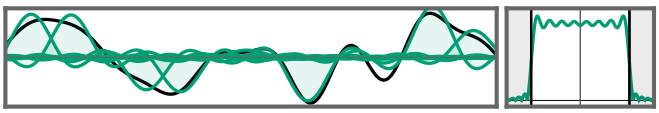

Figure 2: Sinc basis. Left: The same example pulse as in Fig. 1 (black) decomposed with sinc basis elements (green). Right: Spectrum of a basis element with $s = 0.5T$. The vertical lines indicate $\pm\omega_{\max}$. The cut-off at the start and end time of the pulse leads to the spillage to higher frequencies.

C. Sigmoid

The sigmoid basis [13, 33] is composed of smooth time steps, see Fig. 3. The randomised superparameter corresponds to the time of the step. The amplitude A of each step is optimised together with an initial amplitude A_0 at time zero. The number of optimisation parameters is $N_{\text{opt}} = N_s + 1$. Each basis element can be written as:

$$f(s, A; t) = \frac{A}{2}\left(1 + \text{erf}\left(\frac{t-s}{\sqrt{2}\sigma}\right)\right), \qquad (5)$$
$$f_0(A_0; t) = f(0, A_0; t).$$

The frequency is limited by setting the width of each step σ:

$$\sigma = \sqrt{\frac{-2\ln\epsilon_{\text{cut}}}{\omega_{\text{max}}^2}}. \qquad (6)$$

The envelope of the pulse spectrum is given by a Gaussian. To limit the frequency in a comparable manner with respect to the other bases, we require the Gaussian envelope to be reduced to $\epsilon_{\text{cut}} = 0.2$ at ω_{max}. See supplementary material for further discussion on the bandwidth limitations.

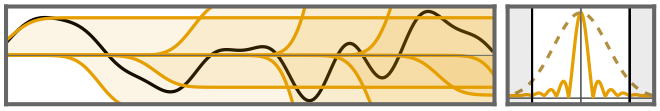

Figure 3: Sigmoid basis. Left: The same example pulse as in Fig. 1 (black) decomposed with sigmoid basis elements (yellow). Right: Spectrum of a basis element with $s = 0.5T$ cut off at beginning and end of the pulse. The vertical lines indicate ω_{max}. The cut-off at the start and end time of the pulse leads to the spillage to higher frequencies. However, sigmoid spectra are on average The dashed line indicates the maximum frequency envelope for an ideal sigmoid pulse (see supplementary material).

III. TEST PROBLEMS

The examples were picked to represent different QOC problems which have previously been shown to be optimisable [16, 29]. Hence, they represent a good point of comparison between different bases. We investigate two factors to evaluate the quality of each basis for a given problem. First, the **convergence probability** P_c, i.e., the percentage of optimisations which converges below a given threshold F_{conv} within a maximum number of function evaluations. Second, the **convergence period** ν_c, i.e., the median of function evaluations needed for the converging optimisations to reach said threshold.

In order for the optimisations to be comparable we set the maximum number of function evaluations to 25 000, use the same number of optimisation parameters N_{opt}, the same pulse time T, and the same maximum frequency ω_{max} for each basis. The hyperparameters, including T and ω_{max}, are chosen to give the best average results for convergence probability. Exemplary results for alternative hyperparameter settings are provided in the supplementary material [34] and show that they do not affect the rankings between the bases. Every optimisation is repeated 2,000 times with different random superparameter s to obtain the average convergence plot. Finally, we investigate common features of the best solutions.

A. Random Ising Chain

The first example is taken in direct analogy to Ref. [16]. Here, the authors showed how an optimisation with the Fourier basis converges depending on the number of optimisation parameters used. Hence, it is an ideal testbed for a comparison with other bases. We consider a chain composed of N spins controlled solely via the global interactions between nearest neighbors with the following Hamiltonian:

$$H_{\text{Is}}/\hbar = \sum_{n=1}^{N} \alpha_n \sigma_n^x + \beta_n \sigma_n^z + c(t) \sum_{n=1}^{N-1} \sigma_n^z \sigma_{n+1}^z. \qquad (7)$$

Each optimisation run is performed with random coefficients $\alpha_i, \beta_i \in [0, 1]$ and random initial and target states, $|\psi_0\rangle$ and $|\psi_t\rangle$. The FoM is given by the final state infidelity

$$J_{\text{Is}} = 1 - |\langle\psi_t| U(T) |\psi_0\rangle|^2, \qquad (8)$$

where $U(T)$ is the time propagator corresponding to Eq (7). The problem becomes harder to solve as the number of qubits N goes up. We have investigated the convergence for $N = \{2, 3, 4\}$. The convergence probabilities P_c, convergence period ν_c, and hyperparameters for the different bases are summarised in Table I.

N		2	3	4
T		20	20	75
ω_{max}		$2\pi 20$	$2\pi 20$	$2\pi 75$
N_{opt}		12	16	16
Fourier	P_c	**99.75%**	**96.75%**	**65.05%**
	ν_c	420	3273	22217
sinc	P_c	**99.8%**	**97.25%**	**90.1%**
	ν_c	224	1291	14898
sigmoid	P_c	**99.45%**	**93.5%**	**0%**
	ν_c	771	4410	–

Table I: Ising model optimisations. The hyperparameters for 2, 3, and 4 qubits are accompanied by the convergence probabilities P_c, and convergence periods ν_c for the three tested bases shown in Fig. 4.

In Fig. 4, we show the median convergence traces of the optimisations. The plots identify a clear winner in terms of convergence periods for all N: The sinc basis is fastest, followed by Fourier and eventually sigmoid. For two and three qubits most optimisations reach the threshold $J_{\text{Is}} < 10^{-3}$. Here, the sinc basis is approximately twice as fast as Fourier and three

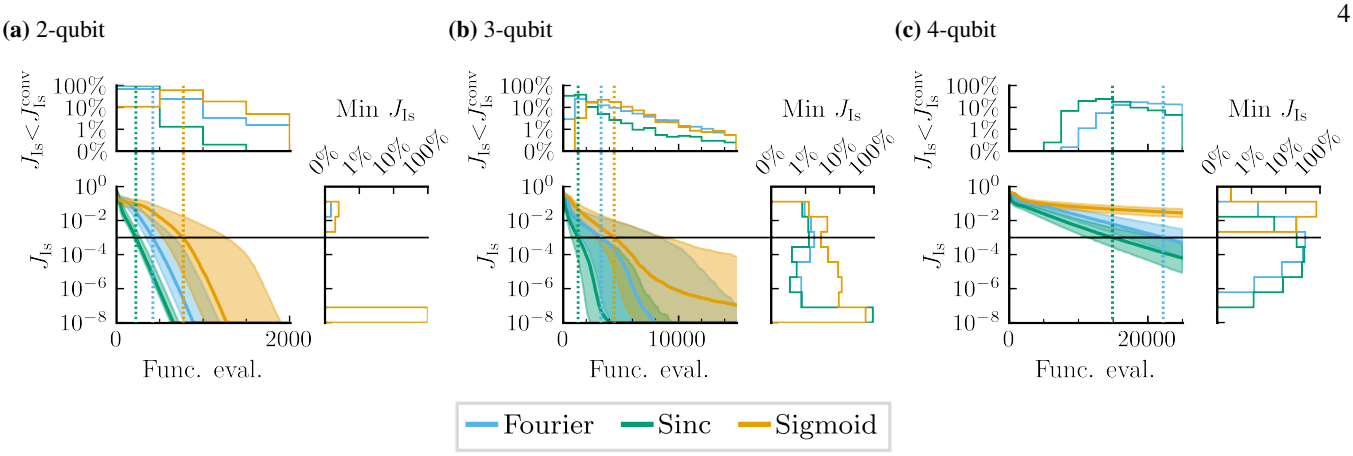

Figure 4: Median convergence of the Ising model problem for 2, 3, and 4 qubits with different bases. The main plots show the median convergence trace with a shaded area representing the 16th and 84th percentiles, i.e. corresponding to 68% of the optimisations. The black horizontal line represents the threshold considered for convergence at $J_{\mathrm{Is}}^{\mathrm{conv}} = 10^{-3}$. The dotted lines show the convergence period ν_c given in Table I. The histograms above represent the percentage of optimisations that have dropped below that threshold within the bin's number of function evaluations. Similarly, the histograms on the right show the final values of the cost J_{Is}. All optimisations were stopped at 10^{-8} or at 25000 iterations.

times as fast as sigmoid. For four qubits more iterations would have been necessary to see convergence for the sigmoid basis while Fourier and sigmoid converge for a majority of optimisations. The average spectra of the converged pulses in Fig. 5 show the big difference between the bases: While the Fourier and sinc basis result in broad spectra with a reduced amplitude at frequency zero, the sigmoid basis remains strongly focused on zero. This result is not surprising as the complexity of building a pulse with a strong frequency component solely with step functions becomes higher for higher frequencies. The absence of high frequency components may be responsible for the sigmoid basis' poor performance for this test problem.

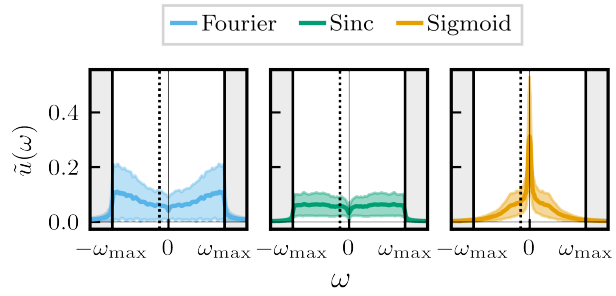

Figure 5: Solutions of the 3-qubit Ising problem: Average spectra for the converged solutions ($J_{\mathrm{Is}} < 10^{-3}$) with different bases. The vertical lines indicate $\omega_{\max}$.

B. Single Qubit Gate on a Qutrit

Most qubit systems are constructed by isolating two levels from a many-level Hamiltonian. One example can be found in NV (nitrogen-vacancy) centers in diamond [35], where the native three-level system is reduced to two, even if at low magnetic field one has to take all three levels into account [36]. Another popular representative are superconducting circuits which can be approximated as qubits due to their anharmonicity Δ. The anharmonicity describes the degree to which the system deviates from a simple harmonic oscillator and hence, how far detuned the $|1\rangle \leftrightarrow |2\rangle$ transition is from the $|0\rangle \leftrightarrow |1\rangle$ transition. Without it, it would not be possible to address the levels separately. Still, even with anharmonicity the transitions are typically close which can lead to leakage and errors in single qubit gates. A number of strategies exists to avoid this issue [37–39] the most famous of which is likely DRAG [29]. This analytic strategy provides controls that prevent a majority of leakage and is explained in further detail in the supplementary material [40]. In zeroth order it reduces the frequency component at Δ majorly responsible for the unwanted coupling to zero. However, QOC methods – specifically the gradient-based method GRAPE – have been shown to outperform it with few parameters [29]. A piecewise-constant basis has even been applied recently to optimise a DRAG-based NOT gate in closed-loop using superconducting qubits [12].

After the application of the rotating wave approximation the three-level system is described by the following Hamiltonian:

$$H_{\mathrm{qb}}/\hbar = \Delta\,|2\rangle\langle 2| + \delta(t)\,|1\rangle\langle 1| + \sum_{n=1,2} \frac{\sqrt{n}}{2}\left[c_x(t)\sigma^x_{n-1,n} + c_y(t)\sigma^y_{n-1,n}\right], \tag{9}$$

where c_x and c_y are the controls on $\sigma_x^{n,m} = |n\rangle\langle m| + |m\rangle\langle n|$, $\sigma_y^{n,m} = i(|m\rangle\langle n| - |n\rangle\langle m|)$, and δ represents the detuning of

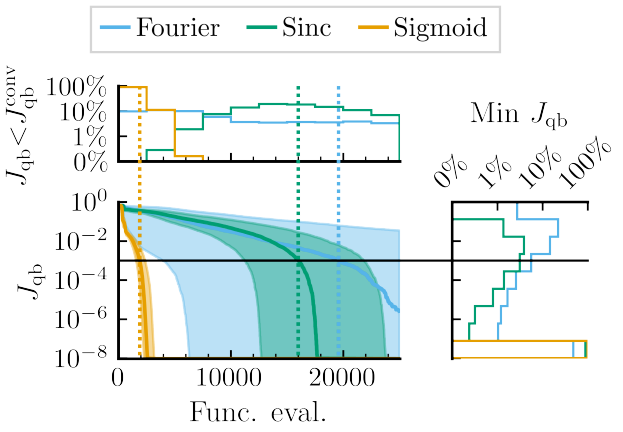

Figure 6: Convergence with different bases optimising a qubit NOT gate. The main plot shows the median convergence trace with a shaded area representing the 16th and 84th percentiles. The histogram on the right shows the distribution over the final FoM, either at 10^{-8} or after 25000 iterations. All optimisations that reach the threshold $J_{qb}^{conv} = 10^{-3}$, represented by the black line, are considered converged. The percentage of optimisations that are converged within the number of iterations are illustrated in the histogram above.

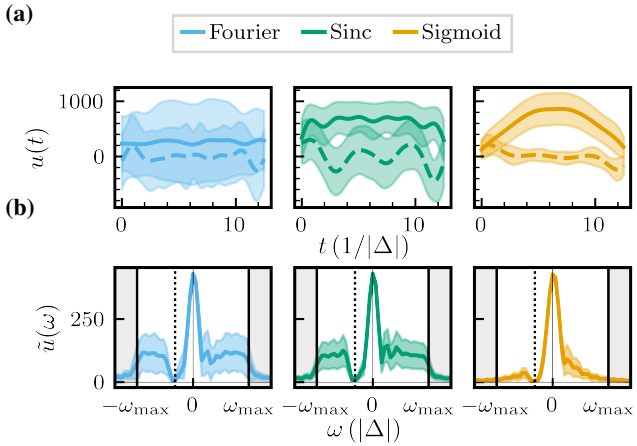

Figure 7: **(a)** Average pulse for the converged solution for different bases. The X and Y pulses are the solid and dashed lines respectively. **(b)** Corresponding average spectra. The solid vertical lines indicate ω_{max} and the dashed line Δ.

the controls. In the following optimisation, $\delta = 0$ and only the x- and y-components of the drive are considered, since a gradual phase change between the components also leads to an effective detuning. The factors $\sqrt{n}$ represent the couplings between the different levels. To calculate the qubit gate fidelity we average over the evolution of all qubit input states $j_{in} = \{\pm x, \pm y, \pm z\}$ lying on the axes of the Bloch sphere. The gate infidelity is then given by [29]

$$J_{qb} = 1 - \frac{1}{6} \sum_{j=j_{in}} \left| \langle j | U_t^\dagger U(T) | j \rangle \right|^2 , \tag{10}$$

where $U(T)$ is the propagator corresponding to Eq (9) at final time T and U_t is the target gate defined as

$$U_t = \begin{pmatrix} 0 & 1 & 0 \\ 1 & 0 & 0 \\ 0 & 0 & 1 \end{pmatrix}. \tag{11}$$

Table II summarises the optimisation results from different bases shown in Fig. 6. The convergence traces indicate that this problem is most efficiently solved with the sigmoid basis. Indeed, the corresponding optimisation is approximately 10 times faster than the other two. The good results are not unexpected as the sigmoid basis can be seen as a dCRAB version of the piecewise-constant basis which has been shown to perform well for this problem [12, 29]. More details on their equivalence can be found in the supplementary material [41]. While the convergence period is similar between the sinc and Fourier basis, the sample variance between Fourier optimisations is large in comparison to the sinc basis. Practically, that means one is more likely to find a good result with the Fourier basis after few iterations than with the sinc basis. However, the probability is also higher to not find a solution at all. This circumstance is illustrated by the top histogram in Fig. 6 and the large spread of the shaded blue area.

The differences between these results can be explained with the average solutions displayed in Fig. 7 considering the properties a good solution should have. A pulse that flips a qubit in presence of a third level without leakage requires two things: an integral equal to π and a hole in its spectrum corresponding to the transition to the third level. The average spectra of the converged pulses in Fig. 7b show exactly that for all bases. Further information is revealed when comparing the time-dependent pulse shapes to DRAG [29]. This analytical strategy for finding leakage-free pulses [42] typically starts with a symmetric x-component of the pulse, while the y-component is antisymmetric following the x-component's derivative. Such behaviour is clearly mirrored in the average sigmoid pulse in Fig. 7a, but less so for the other two bases. After all, the sigmoid basis only requires one element to build a low-bandwidth, high integral x-pulse, and only two for a low-frequency, antisymmetric y-pulse. For both Fourier and sinc basis such a construction is more complex. Especially the sinc basis has a naturally wide spectrum, leading to large

Basis	P_c	ν_c
Fourier	**57.64%**	19567
sinc	**93.44%**	15987
sigmoid	**99.96%**	1880

Table II: Convergence probabilities and speeds for the NOT gate using hyperparameters $T = 12.5/|\Delta|$, $N_{opt} = 6$, and $\omega_{max} = 12.5\pi/|\Delta|$ with $\Delta = -400 \cdot 2\pi$ MHz chosen to produce efficient optimisations.

leakage unless it is actively counteracted, which explains the slow convergence.

IV. DISCUSSION

The set of existing QOC methods unites different approaches: some gradient-free, some gradient-based, some including an inherent modelling technique, and others relying on black boxes. They all have the common goal to efficiently optimise quantum processes with the given resources. In general, using fewer parameters typically leads to a smaller search space and hence quicker convergence. However, the solutions are bad if the smaller search space does not include a good optimum. Changing the basis functions could be seen as an adjustment of the search space: With the right basis set, fewer parameters are required to find a good solution. Hence, the convergence is sped up.

This interpretation is supported by our results. In some cases, like the single qubit gate in Sec. III B, we can clearly identify the characteristics of a good solution. The average converged pulses, as well as the average spectra, show specific properties that are more complex to produce with the Fourier and sinc bases than sigmoid or piecewise-constant. Similarly, broad spectra require many more sigmoid elements than Fourier or sincfunctions as shown on Sec. III A. **Hence, a basis which reproduces known solutions to similar problems with few elements constitutes a promising choice.** In other cases, like the Ising model problem described in Sec. III A, no such recipe exists making the QOC application even more relevant. Still, in this example we can see that the ranking between the bases does not change with rising qubit number for the same problem class. Assuming that this transferability applies to other problems as well it allows for a cheap way to test for the best basis choice: **The best basis for a problem may be indicated by a test on a simplified version of the problem.**

V. CONCLUSION

The optimisation of different problems with different bases shows that the convergence period depends on the applied set of basis functions, with differences of up to a factor of 10 in the number of function evaluations required. For the presented examples, the ranking between the bases is dependent on the problem they are applied to. However, the ranking does not change with the problem complexity, see the number of qubits in the Ising model.

The convergence plots suggest that an educated choice of basis elements is likely to outperform the default, when attempting to reduce the number of basis elements. This is often the case for closed-loop optimisations, as most gradient-free optimisers are more effective in smaller search spaces and experimental evaluations are expensive. The right basis may lead to a faster and better solution with higher success probability. The basis choice should consider the decomposition of known solutions for similar problems or through trial-runs with a lower-complexity version of the problem (e.g., less qubits/energy levels or model-based open-loop).
In a situation where the required properties are well-known, they could be encoded directly into the optimisation for the cost of restricting the search space. A suggestion for such an approach for DRAG-criteria is given in the supplementary material [43].

VI. OUTLOOK

Thinking ahead, if one basis can outperform the other, what could their combination achieve? Especially in situations where no clear basis candidates present themselves, combining bases might be a valid strategy to explore. They could either be combined simultaneously, added in subsequent superiterations, or by creating hybrid bases, e.g., sincs with different bandwidths or frequency elements cut off by sigmoids. Our investigations only covered an exemplary set of bases, but others like the Slepian [44], Walsh [45] windowed Gaussian [28], or B-spline [46] basis might offer further advantages. Furthermore, the presented results were produced with gradient-free dCRAB and partially confirmed with AD-based CRAB [47]. We would be interested to see whether they hold as expected for other basis-flexible optimisation methods like GOAT and GROUP. In summary, we show how the basis choice affects the efficiency of optimisations and hope that our conclusions will inspire the use of a larger range of basis functions.

Code and data availability – The code to perform the optimal control is available as QuOCS [31]. The code for the analysis is available upon reasonable request. All the figures are available at [48].

ACKNOWLEDGMENTS

PR thanks Ian Yang, Robert Zeier, and Yuri Minoguchi for useful discussions. AP thanks Daniel Jaschke for useful discussions. This project has received funding from the German Federal Ministry of Education and Research (BMBF) under the funding program quantum technologies – from basic research to market – with the grant QRydDemo. We acknowledge financial support from the Italian Ministry of University and Research (MUR) via the Department of Excellence grant 2023-2027 Quantum Frontiers; from the European Union via H2020 projects EuRyQa, TEXTAROSSA, and the Quantum Flagship project Pasquans2, the EU-QuantERA projects QuantHEP and T-NISQ, and from the World Class Research Infrastructure – Quantum Computing and Simulation Center (QCSC) of Padova University, and the Italian National Centre on HPC, Big Data and Quantum Computing. The authors acknowledge support by the state of Baden-Württemberg through bwHPC and the German Research Foundation (DFG) through grant no INST 40/575-1 FUGG (JUSTUS 2 cluster). We acknowledge funding within the HPQC project by the Austrian Research Promotion Agency (FFG, project number 897481) supported

by the European Union – NextGenerationEU. We acknowledge HORIZON-CL4-2022-QUANTUM-01-SGA project under Grant 101113946 OpenSuperQ- Plus100, by Germany's Excellence Strategy – Cluster of Excellence Matter and Light for Quantum Computing (ML4Q) EXC 2004/1 – 390534769, by the Helmholtz Validation Fund project "Qruise" (HVF-00096), and by the German Federal Ministry of Research (BMBF) under the project SPINNING (No. 13N16210), PASQUANS2.

[1] C. P. Koch, U. Boscain, T. Calarco, G. Dirr, S. Filipp, S. J. Glaser, R. Kosloff, S. Montangero, T. Schulte-Herbrüggen, D. Sugny, and F. K. Wilhelm, Quantum optimal control in quantum technologies. strategic report on current status, visions and goals for research in europe, EPJ Quantum Technology **9**, 10.1140/epjqt/s40507-022-00138-x (2022).

[2] S. J. Glaser, U. Boscain, T. Calarco, C. P. Koch, W. Köckenberger, R. Kosloff, I. Kuprov, B. Luy, S. Schirmer, T. Schulte-Herbrüggen, D. Sugny, and F. K. Wilhelm, Training schrödinger's cat: quantum optimal control: Strategic report on current status, visions and goals for research in europe, The European Physical Journal D **69**, 10.1140/epjd/e2015-60464-1 (2015).

[3] C. Brif, R. Chakrabarti, and H. Rabitz, Control of quantum phenomena: past, present and future, New Journal of Physics **12**, 075008 (2010).

[4] P. Rembold, N. Oshnik, M. M. Müller, S. Montangero, T. Calarco, and E. Neu, Introduction to quantum optimal control for quantum sensing with nitrogen-vacancy centers in diamond, AVS Quantum Science **2**, 024701 (2020).

[5] M. M. Müller, R. S. Said, F. Jelezko, T. Calarco, and S. Montangero, One decade of quantum optimal control in the chopped random basis, Reports on Progress in Physics **85**, 076001 (2022).

[6] A. Omran, H. Levine, A. Keesling, G. Semeghini, T. T. Wang, S. Ebadi, H. Bernien, A. S. Zibrov, H. Pichler, S. Choi, J. Cui, M. Rossignolo, P. Rembold, S. Montangero, T. Calarco, M. Endres, M. Greiner, V. Vuletić, and M. D. Lukin, Generation and manipulation of schrödinger cat states in rydberg atom arrays, Science **365**, 570–574 (2019).

[7] A. Pagano, S. Weber, D. Jaschke, T. Pfau, F. Meinert, S. Montangero, and H. P. Büchler, Error budgeting for a controlled-phase gate with strontium-88 rydberg atoms, Physical Review Research **4**, 10.1103/physrevresearch.4.033019 (2022).

[8] S. Rosi, A. Bernard, N. Fabbri, L. Fallani, C. Fort, M. Inguscio, T. Calarco, and S. Montangero, Fast closed-loop optimal control of ultracold atoms in an optical lattice, Physical Review A **88**, 10.1103/physreva.88.021601 (2013).

[9] S. van Frank, M. Bonneau, J. Schmiedmayer, S. Hild, C. Gross, M. Cheneau, I. Bloch, T. Pichler, A. Negretti, T. Calarco, and S. Montangero, Optimal control of complex atomic quantum systems, Scientific Reports **6**, 10.1038/srep34187 (2016).

[10] R. Heck, O. Vuculescu, J. J. Sørensen, J. Zoller, M. G. Andreasen, M. G. Bason, P. Ejlertsen, O. Elíasson, P. Haikka, J. S. Laustsen, L. L. Nielsen, A. Mao, R. Müller, M. Napolitano, M. K. Pedersen, A. R. Thorsen, C. Bergenholtz, T. Calarco, S. Montangero, and J. F. Sherson, Remote optimization of an ultracold atoms experiment by experts and citizen scientists, Proceedings of the National Academy of Sciences **115**, 10.1073/pnas.1716869115 (2018).

[11] P. Cerfontaine, T. Botzem, J. Ritzmann, S. S. Humpohl, A. Ludwig, D. Schuh, D. Bougeard, A. D. Wieck, and H. Bluhm, Closed-loop control of a gaas-based singlet-triplet spin qubit with 99.5% gate fidelity and low leakage, Nature Communications **11**, 10.1038/s41467-020-17865-3 (2020).

[12] M. Werninghaus, D. J. Egger, F. Roy, S. Machnes, F. K. Wilhelm, and S. Filipp, Leakage reduction in fast superconducting qubit gates via optimal control, npj Quantum Information **7**, 1 (2021), number: 1 Publisher: Nature Publishing Group.

[13] N. Oshnik, P. Rembold, T. Calarco, S. Montangero, E. Neu, and M. M. Müller, Robust magnetometry with single nitrogen-vacancy centers via two-step optimization, Physical Review A **106**, 013107 (2022), publisher: American Physical Society.

[14] P. J. Vetter, T. Reisser, M. G. Hirsch, T. Calarco, F. Motzoi, F. Jelezko, and M. M. Müller, Gate-set evaluation metrics for closed-loop optimal control on nitrogen-vacancy center ensembles in diamond (2024), arXiv:2403.00616 [quant-ph].

[15] T. Caneva, T. Calarco, and S. Montangero, Chopped random-basis quantum optimization, Physical Review A - Atomic, Molecular, and Optical Physics **84**, 22326 (2011), arXiv: 1103.0855.

[16] N. Rach, M. M. Müller, T. Calarco, and S. Montangero, Dressing the chopped-random-basis optimization: A bandwidth-limited access to the trap-free landscape, Physical Review A **92**, 10.1103/physreva.92.062343 (2015).

[17] S. Machnes, E. Assémat, D. Tannor, and F. K. Wilhelm, Tunable, Flexible, and Efficient Optimization of Control Pulses for Practical Qubits, Physical Review Letters **120**, 150401 (2018).

[18] N. Khaneja, T. Reiss, C. Kehlet, T. Schulte-Herbrüggen, and S. J. Glaser, Optimal control of coupled spin dynamics: design of NMR pulse sequences by gradient ascent algorithms, Journal of Magnetic Resonance **172**, 296 (2005).

[19] See Supplementary Material I.

[20] A. I. Konnov and V. F. Krotov, On global methods for the successive improvement of control processes, Avtomatika i Telemekhanika **60**, 77 (1999).

[21] J. J. W. H. Sørensen, M. O. Aranburu, T. Heinzel, and J. F. Sherson, Quantum optimal control in a chopped basis: Applications in control of Bose-Einstein condensates, Physical Review A **98**, 022119 (2018), publisher: American Physical Society.

[22] F. Motzoi, J. M. Gambetta, S. T. Merkel, and F. K. Wilhelm, Optimal control methods for rapidly time-varying Hamiltonians, Physical Review A **84**, 022307 (2011), publisher: American Physical Society.

[23] S. Lloyd and S. Montangero, Information theoretical analysis of quantum optimal control, Physical Review Letters **113**, 1 (2014), arXiv: 1401.5047.

[24] T. Caneva, A. Silva, R. Fazio, S. Lloyd, T. Calarco, and S. Montangero, Complexity of controlling quantum many-body dynamics, Physical Review A **89**, 10.1103/physreva.89.042322 (2014).

[25] M. M. Müller, S. Gherardini, T. Calarco, S. Montangero, and F. Caruso, Information theoretical limits for quantum optimal control solutions: error scaling of noisy control channels, Scientific Reports **12**, 10.1038/s41598-022-25770-6 (2022).

[26] J. H. M. Jensen, F. S. Møller, J. J. Sørensen, and J. F. Sherson, Achieving fast high-fidelity optimal control of many-body quantum dynamics, Physical Review A **104**, 052210 (2021).

[27] X. Li, Optimal control of quantum state preparation and entanglement creation in two-qubit quantum system with bounded amplitude, Scientific Reports **13**, 14734 (2023), publisher: Nature Publishing Group.

[28] T. Chalermpusitarak, B. Tonekaboni, Y. Wang, L. M. Norris, L. Viola, and G. A. Paz-Silva, Frame-Based Filter-Function Formalism for Quantum Characterization and Control, PRX Quantum **2**, 030315 (2021).

[29] F. Motzoi, J. M. Gambetta, P. Rebentrost, and F. K. Wilhelm, Simple Pulses for Elimination of Leakage in Weakly Nonlinear Qubits, Phys. Rev. Lett. **103**, 110501 (2009).

[30] See Supplementary Material III.

[31] M. Rossignolo, T. Reisser, A. Marshall, P. Rembold, A. Pagano, P. J. Vetter, R. S. Said, M. M. Müller, F. Motzoi, T. Calarco, F. Jelezko, and S. Montangero, QuOCS: The Quantum Optimal Control Suite, Computer Physics Communications , 108782 (2023).

[32] See Supplementary Material I.

[33] P. Rembold, *Quantum Optimal Control of Spin Systems and Trapped Atoms*, PhD thesis, Universität zu Köln and Università degli Studi di Padova (2022).

[34] See Supplementary Material II.

[35] M. W. Doherty, N. B. Manson, P. Delaney, F. Jelezko, J. Wrachtrup, and L. C. L. Hollenberg, The nitrogen-vacancy colour centre in diamond, Physics Reports The nitrogen-vacancy colour centre in diamond, **528**, 1 (2013).

[36] P. J. Vetter, A. Marshall, G. T. Genov, T. F. Weiss, N. Striegler, E. F. Großmann, S. Oviedo-Casado, J. Cerrillo, J. Prior, P. Neumann, and F. Jelezko, Zero- and low-field sensing with nitrogen-vacancy centers, Phys. Rev. Appl. **17**, 044028 (2022).

[37] P. Krantz, M. Kjaergaard, F. Yan, T. P. Orlando, S. Gustavsson, and W. D. Oliver, A quantum engineer's guide to superconducting qubits, Applied Physics Reviews **6**, 10.1063/1.5089550 (2019), arXiv: 1904.06560 Publisher: AIP Publishing LLC.

[38] T. Caneva, M. Murphy, T. Calarco, R. Fazio, S. Montangero, V. Giovannetti, and G. E. Santoro, Optimal Control at the Quantum Speed Limit, Physical Review Letters **103**, 240501 (2009).

[39] S. Safaei, S. Montangero, F. Taddei, and R. Fazio, Optimized single-qubit gates for josephson phase qubits, Physical Review B **79**, 10.1103/physrevb.79.064524 (2009).

[40] See Supplementary Material V.

[41] See Supplementary Material I.

[42] See Supplementary Material V.

[43] See Supplementary Material V.

[44] D. Lucarelli, Quantum optimal control via gradient ascent in function space and the time-bandwidth quantum speed limit, Physical Review A **97**, 062346 (2018).

[45] D. Hayes, K. Khodjasteh, L. Viola, and M. J. Biercuk, Reducing sequencing complexity in dynamical quantum error suppression by Walsh modulation, Physical Review A **84**, 062323 (2011), publisher: American Physical Society.

[46] S. Günther, N. A. Petersson, and J. L. DuBois, Quantum optimal control for pure-state preparation using one initial state, AVS Quantum Science **3**, 043801 (2021).

[47] See Supplementary Material III.

[48] A. Pagano, M. M. Müller, T. Calarco, S. Montangero, and P. Rembold, Figures and supplementary material of The Role of Bases in Quantum Optimal Control, Figshare 10.6084/m9.figshare.c.7277647.v2 (2024).

Supplemental Material – The Role of Bases in Quantum Optimal Control

Alice Pagano,[1,2,3] Matthias M Müller,[4] Tommaso Calarco,[4,5,6] Simone Montangero,[1,2,3] and Phila Rembold[2,5,7]

[1]*Institute for Complex Quantum Systems, Ulm University, Albert-Einstein-Allee 11, 89069 Ulm, Germany*

[2]*Dipartimento di Fisica e Astronomia "G. Galilei" & Padua Quantum Technologies Research Center, Università degli Studi di Padova, 35131 Padova, Italy*

[3]*INFN, Sezione di Padova, via Marzolo 8, 35131 Padova, Italy*

[4]*Peter Grünberg Institute – Quantum Control (PGI-8), Forschungszentrum Jülich GmbH, 52425 Jülich, Germany*

[5]*Institute for Theoretical Physics, University of Cologne, 50937 Köln, Germany*

[6]*Dipartimento di Fisica e Astronomia, Università di Bologna, 40127 Bologna, Italy*

[7]*Atominstitut, Technische Universität Wien, Stadionallee 2, 1020 Wien, Austria*

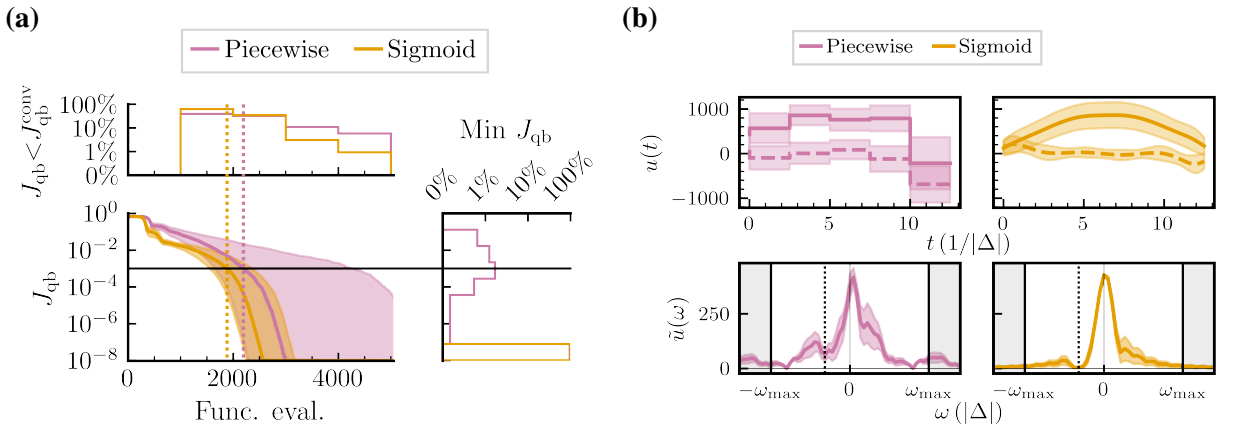

Figure 1: **(a)** Comparison between sigmoid and piecewise basis for qutrit problem. The convergence probability for the piecewise is $P_c = 97.6\%$, the one for the sigmoid is $P_c = 99.96\%$ as reported in the main text. The number of parameters optimized is $N_c = 6$. **(b)** Pulse and spectrum comparison.

I. THE PIECEWISE-CONSTANT BASIS

Many algorithms commonly apply the piece-wise constant basis. Their most prominent representatives are GRAPE [1] and Krotov's method [2], both of which are gradient-based open-loop optimisation methods. The sigmoid basis represents the same function-space as the piece-wise constant basis, if the sigmoid width is $\sigma \ll 1$ creating genuine step functions. In general, all basis elements are considered to be of the same length for the piecewise-constant basis which is taken into consideration by

$$\tau_p = \tau_0 + p\Delta\tau, \text{ where } \Delta\tau = \frac{\tau_N - \tau_0}{N}. \tag{1}$$

The parameter scaling the p^{th} sigmoid basis element is given by A_p. Similarly, the k^{th} piece-wise constant element is scaled by $u^{(k)}$ in analogy to GRAPE, where $u^{(0)} = u^{(N+1)} = 0$. Assuming that $\sigma \ll \Delta\tau$, they are connected by the following relationships:

$$\begin{aligned} A_p &= u^{(p+1)} - u^{(p)}, \\ u^{(k)} &= \sum_{p=0}^{k-1} A_p. \end{aligned} \tag{2}$$

To see how this transformation may be exploited in a gradient-based context, please refer to Ref. [3]. The example problem presented in Sec. IIIB is known to be well optimisable using the piecewise-constant basis [4]. To show that the sigmoid basis is not only in principle equivalent but also a sensible replacement, we compare the two bases in Fig. 1 for the NOT gate optimization.

II. HYPERPARAMETERS

The selected hyperparameters for the test problems in Sec. III are representative and aim to yield the best average results for convergence probability. To demonstrate this, in the following we show that varying the hyperparameters does not alter the results.

In Fig. 2, the convergence traces for a different set of hyperparameters for different number of qubits are reported. The parameters are assumed to be the one fixed in Table I unless stated differently on top of the plot. In more detail, we present the results for two qubits with varying final times T, for three qubits with different numbers of optimization parameters N_{opt} and for four qubits with different maximum frequencies ω_{max}. By examining the results, as summarized in Table I, we confirm that for this problem, the sinc basis converges faster than the Fourier basis, and the sigmoid basis does not perform well.

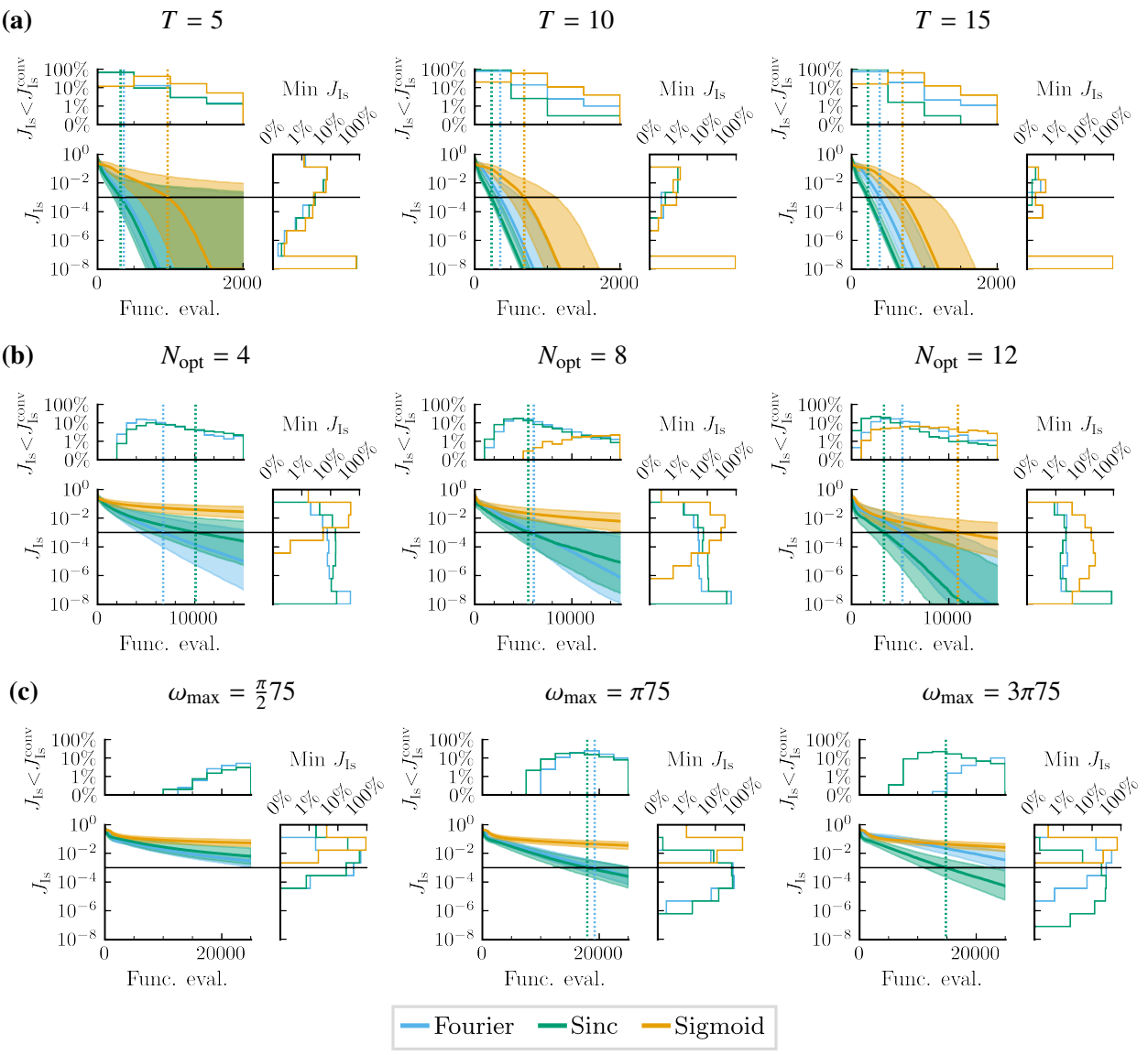

Figure 2: Comparing convergence traces with varying hyperparameters. (a) 2-qubit analysis involves changes in the final time T (b) 3-qubit analysis focuses on variations in optimization parameters N_{opt} (c) 4-qubit analysis explores variations in the maximum frequency ω_{max}.

For the single qubit gate problem, we compare the histogram in Fig. 3 showing the percentage of optimizations that have converged below different thresholds as a function of the number of iterations, particularly for $J_{\text{qb}}^{\text{conv}} = \{10^{-6}, 10^{-4}, 10^{-2}\}$. The quicker convergence rate of the sigmoid basis method remains consistent across all thresholds.

N		2			3			4		
T		5	10	15	20			75		
$\omega_{\max}$		$2\pi 20$			$2\pi 20$			$\frac{\pi}{2}75$	$\pi 75$	$3\pi 75$
N_{opt}		12			4	8	12	16		
Fourier	P_c	**84.85%**	**97.85%**	**99.45%**	**89.5%**	**93.2%**	**95.85%**	**12.5%**	**83.05%**	**22.45%**
	ν_c	362	351	386	6749	6084	5234	–	19219	–
sinc	P_c	**83.85%**	**98.05%**	**99.5%**	**78.5%**	**91.05%**	**96.25%**	**7.95%**	**81.6%**	**89.6%**
	ν_c	316	230	225	10086	5509	3338	–	17964	14794
sigmoid	P_c	**82.9%**	**97.85%**	**99.2%**	**1.85%**	**32.0%**	**79.7%**	**0%**	**0%**	**0%**
	ν_c	963	681	700	–	–	10939	–	–	–

Table I: For 2, 3, and 4 qubits, the hyperparameters are associated with convergence probabilities P_c and convergence periods ν_c for the three bases tested.

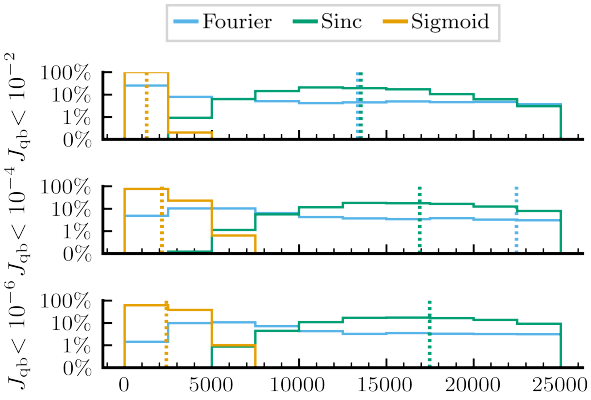

Figure 3: Comparison of the histograms representing the percentage of optimizations that have reached various cutoff thresholds ($J_{\text{qb}}^{\text{conv}}$) for the single qubit gate problem.

III. AUTOMATIC DIFFERENTIATION

To show that our analysis is independent of the optimisation method, we confirm the results from the Ising chain with an AD-based optimisation. AD allows the calculation of gradients directly from the code [5, 6]. The optimisation was implemented using the JAX library [7] in python and hyperparameters specified in Table II. The number of parameters was chosen to be

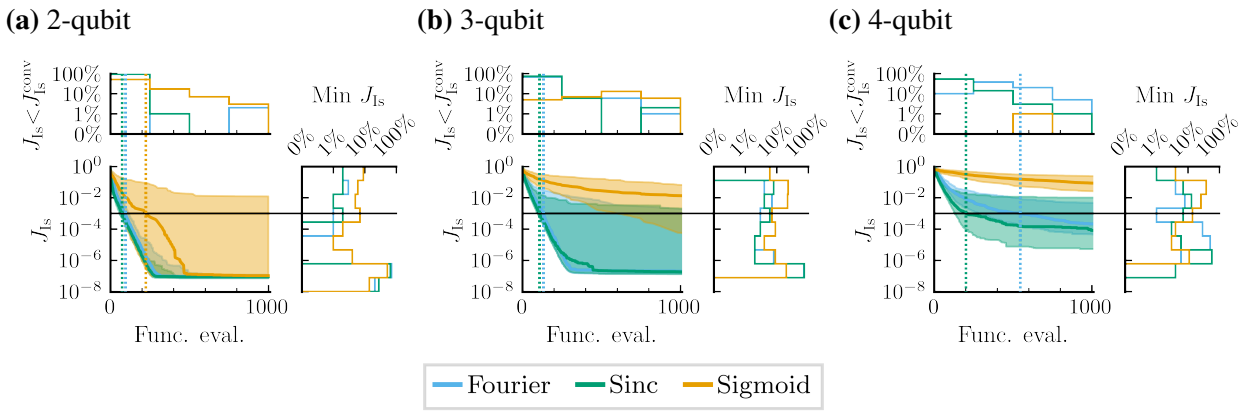

Figure 4: Ising chain convergence traces with AD for 100 different optimisations for 2, 3, and 4 qubits respectively. The main plot show the median convergence trace. The black horizontal line represents the threshold at 10^{-3}. The histogram above is the percentage of optimisations that have dropped below the threshold within the number of iterations. Similarly, the histogram on the right show the final value of the cost function. All optimisations were stopped at 10^{-7}.

twice as high for the sigmoid basis as it provides better convergence and is feasible with the applied gradient-based updating algorithm ADAM [8]. In this framework, we optimise the parameters as well as the superparameters to make a point of not using dCRAB. This is possible as ADAM imposes fewer restrictions on the number of parameters.

The results in Fig. 4 show that the Fourier and sinc bases outperform the sigmoid basis, even though the ladder is provided with a higher number of parameters. The results confirm the speedup in convergence of the sinc basis, especially in the case of four qubits as summarized in Table II. The optimisation is repeated 100 times.

IV. SIGMOID BASIS

We consider the pulse basis elements $f(t)$ to be sigmoid functions. Sigmoids can in general be defined as the integral of a function with a single maximum at the centre. For the sake of simplicity, we only consider the sigmoid function that is defined by the integral of a Gaussian defined as

$$\begin{aligned} f(t) &= \frac{A_p}{\sqrt{2\pi}\sigma} \int_{-\infty}^{t} e^{-\frac{1}{2}\left(\frac{t'-\tau_p}{\sigma}\right)^2} dt' \\ &= \frac{A_p}{2}\left(1 + \mathrm{erf}\left(\frac{t-\tau_p}{\sqrt{2}\sigma}\right)\right). \end{aligned} \tag{3}$$

N		2	3	4
T		15	20	75
$\omega_{\max}$		2π	2π	4π
Fourier	N_{opt}	24	30	30
	P_c	**94.0%**	**87.0%**	**86.0%**
	ν_c	95	133	546
sinc	N_{opt}	24	30	30
	P_c	**95.0%**	**86.0%**	**76.0%**
	ν_c	74	108	201
sigmoid	N_{opt}	48	60	60
	P_c	**78.0%**	**45.0%**	**24.0%**
	ν_c	224	–	–

Table II: Ising chain optimisation performed with AD for 2, 3, and 4 qubits. The hyperparameters were empirically chosen to improve the convergence period. They are displayed together with the convergence probability P_c, and convergence period ν_c for the three tested bases.

Each element is characterised by the amplitude A_p of the Gaussian, the centre time τ_p and the width σ. Accordingly, the sigmoid function resembles a smooth step function going from 0 to A_p at a time τ_p. Restrictions on the first derivative and hence rise time and bandwidth can be enforced via σ. As an example, to limit the gradient to that of a linear ramp of length t_{rise} from 0 to $A_{\max}$ one should set $\sigma \geq \sqrt{2/\pi}\ t_{\text{rise}}$. The difference made by the choice of σ is illustrated in Fig. 5. Similarly, we can restrict the pulse length and amplitude via A_p and τ_p as discussed in Ref. [3].

The sigmoid basis is composed of spectrally narrow elements with a time-limited derivative. As a result its bandwidth envelope is predictable. The spectrum of a pulse $u(t)$ constructed from a time-limited sum of N sigmoid elements reads

$$\mathcal{F}[u(t)] = \frac{1}{i\omega} e^{-\frac{1}{2}\sigma^2\omega^2} \sum_{p=0}^{N} A_p e^{i\tau_p\omega}. \tag{4}$$

From this expression, one can derive a bandwidth envelope for any constructible pulse, which is only dependent on σ, $A_{\max}$, the first rise time τ_0, and the maximal rise time τ_N. To do so, we consider the pulse with the highest possible integral, i.e. a square pulse with amplitude $A_{\max}$. As the integral corresponds to the zero-frequency component of the spectrum and the pulse is

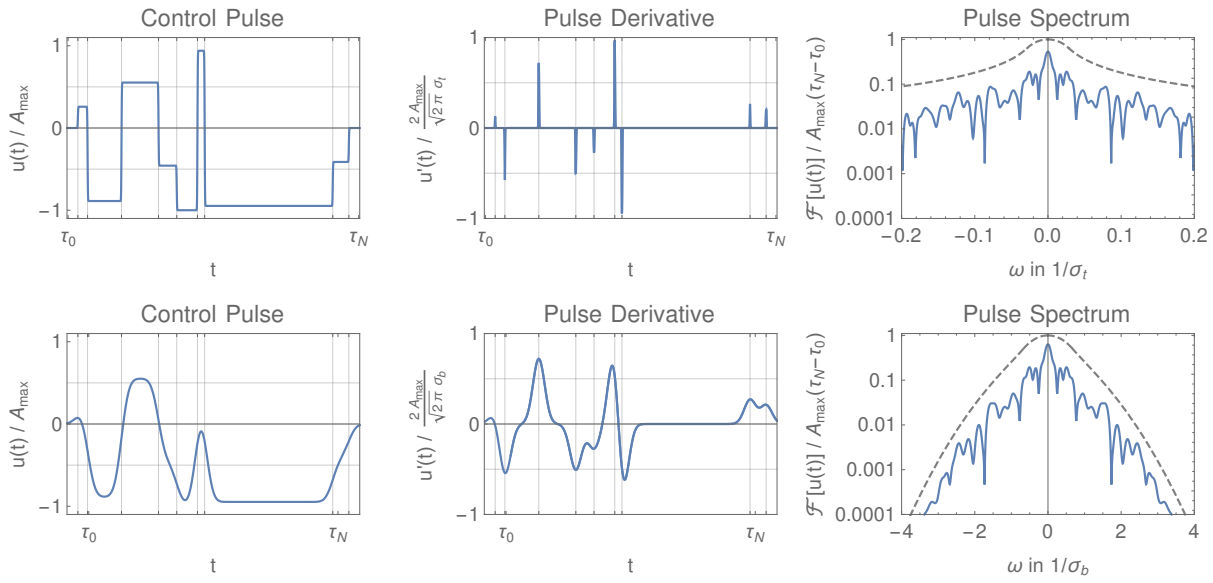

Figure 5: The effect of σ. From left to right, one can see apulse composed via the sigmoid basis, its derivative, and its spectrum. The top row shows a pulse constructed using a small width $\sigma_\mathrm{t} = \frac{1}{20}\,\sigma_\mathrm{b}$ while the bottom is made up of elements with σ_b. Please note that the right column is plotted over the same frequency range. The dashed line shows the respective bandwidth envelope. This figure was taken from Ref [3] with the author's permission.

symmetric, we can deduce the amplitude of the bandwidth limiting envelope $Y^{\infty}_{\mathrm{max}}$ shown in Fig. 6,

$$Y^{\infty}_{\mathrm{max}}(\omega) = A_{\mathrm{max}}(\tau_N - \tau_0)\, e^{-\frac{1}{2}\sigma^2\omega^2}. \tag{5}$$

This relation holds for infinitely many basis elements. However, the limit for a pulse constructed from N basis elements is given by

$$\begin{aligned} k &= \frac{(\tau_N - \tau_0)\omega}{2N}, \\ Y^{N}_{\mathrm{max}} &= Y^{\infty}_{\mathrm{max}} \begin{cases} -1/k & k \le -\frac{\pi}{2} \\ \sin k/k & -\frac{\pi}{2} < k < \frac{\pi}{2} \\ +1/k & k \ge \frac{\pi}{2} \end{cases} . \end{aligned} \tag{6}$$

The center part $\mathrm{sinc}(k)$ represents the Fourier transform of a square pulse of length $(\tau_N - \tau_0)/N$. The bandwidth envelope Y^{N}_{max} is shown for different values of N in Fig. 6.

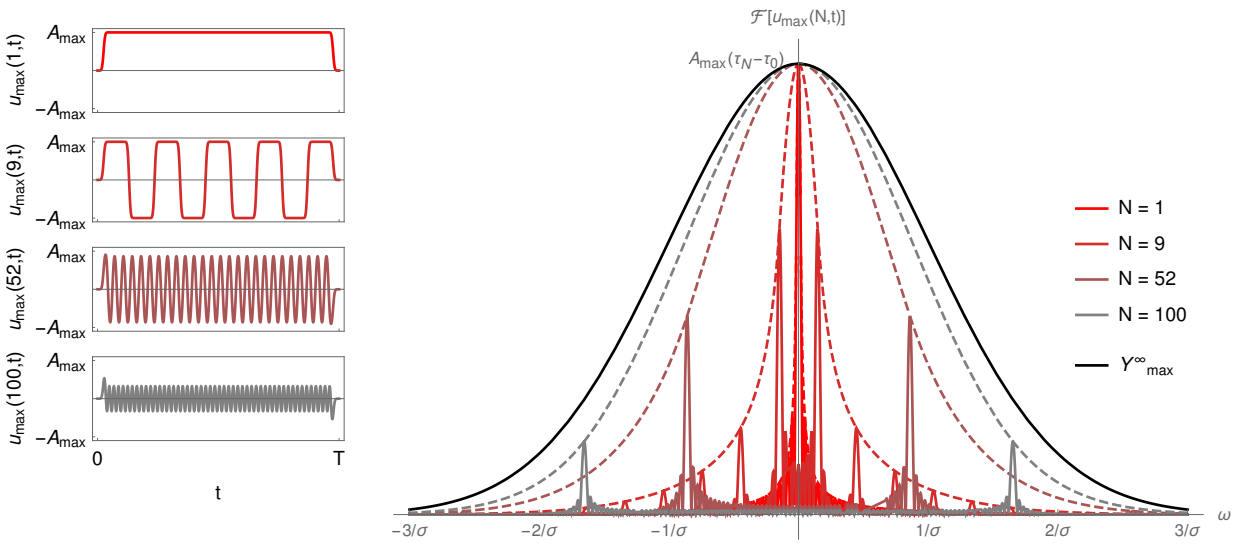

Figure 6: Control pulses composed to be time- and amplitude-limited and their corresponding spectra. The dashed lines represent $Y^N_{\max}$, the solid line gives $Y^{\infty}_{\max}$. This figure was taken from Ref [3] with the author's permission.

V. SIGMOID IN DRAG

In zeroth order, DRAG creates pulses which methodically avoid unwanted transitions at a frequency Δ_0. Here, we suggest a way to directly implement that condition in the pulses during optimisation. Please note that the following Appendix directly follows Ref. [3].

A complex pulse $u(t) = I(t) + iQ(t)$ has an asymmetric spectrum. By exploiting the relationship between the in-phase I-component $I(t)$ and quadrature Q-component $Q(t)$, specific components can be set to zero. First, let us consider a real function $f(t)$ which is limited in time i.e. $f(0) = f(T) = 0$. Its Fourier transform is given by $\mathcal{F}[f(t)] = Y(\omega)$. The Fourier identity for the spectrum of the function's first derivative reads:

$$\begin{aligned} \mathcal{F}[f'(t)] = X(\omega) &= -i\omega Y(\omega) \\ 0 = Y(\omega) &+ i\frac{X(\omega)}{\omega}. \end{aligned} \tag{7}$$

To ensure that the spectrum of the complex pulse $u(t)$ has a node at Δ_0, we can define the pulse components as

$$\begin{aligned} I(t) &= f(t) \text{ and} \\ Q(t) &= -\frac{f'(t)}{\Delta_0}, \end{aligned} \tag{8}$$

making its Fourier transform

$$\begin{aligned}\mathcal{F}[u(t)] &= \mathcal{F}[I(t)] + \mathcal{F}[iQ(t)] \\ &= \mathcal{F}[f(t)] - i\mathcal{F}\left[-\frac{f'(t)}{\Delta_0}\right] \\ &= Y(\omega) + i\frac{X(\omega)}{\Delta_0}.\end{aligned} \tag{9}$$

Combining Eq. (7) and Eq. (9) shows that the Fourier transform is zero at $\omega = \Delta_0$. This effect is illustrated in Fig. 7. With the sigmoid basis, such pulses can be constructed straight-forwardly

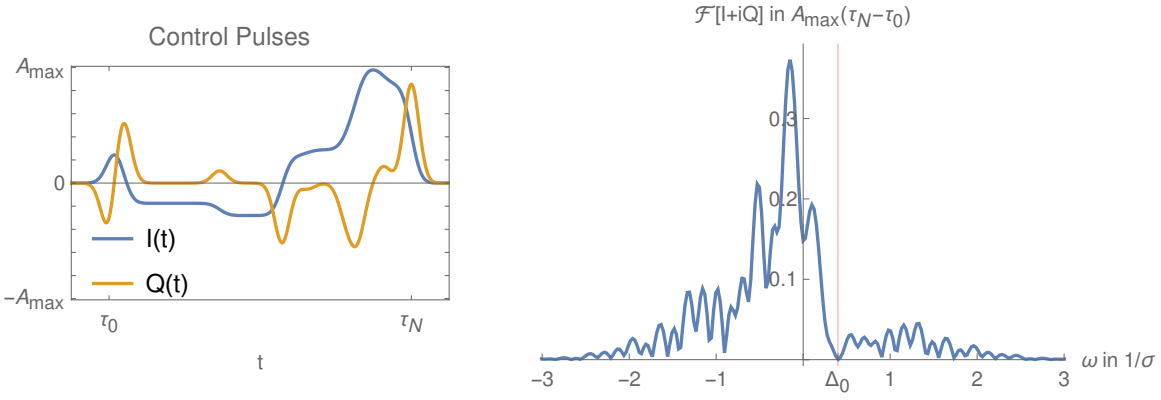

Figure 7: DRAG control pulse constructed with the sigmoid basis. (*left*) I- and Q-component calculated according to eq. (8) with a detuning of Δ_0. (*right*) Pulse spectrum with a distinctive node at Δ_0. This figure was taken from Ref [3] with the author's permission.

resulting in $I(t)$ being made up of sigmoids and $Q(t)$ of Gaussians, i.e. the sigmoids' derivatives. However, a similar approach could be applied to other bases too.

For completeness, it should be mentioned that higher orders of DRAG which include the relationship between the pulse amplitudes and detuning have not been discussed here, but could in principal also be included in such conditions.

---

[1] N. Khaneja, T. Reiss, C. Kehlet, T. Schulte-Herbrüggen, and S. J. Glaser, Optimal control of coupled spin dynamics: design of NMR pulse sequences by gradient ascent algorithms, Journal of Magnetic Resonance **172**, 296 (2005).

[2] A. I. Konnov and V. F. Krotov, On global methods for the successive improvement of control processes, Avtomatika i Telemekhanika **60**, 77 (1999).

[3] P. Rembold, *Quantum Optimal Control of Spin Systems and Trapped Atoms*, PhD thesis, Universität zu Köln and Università degli Studi di Padova (2022).

[4] F. Motzoi, J. M. Gambetta, P. Rebentrost, and F. K. Wilhelm, Simple Pulses for Elimination of Leakage in Weakly Nonlinear Qubits, Phys. Rev. Lett. **103**, 110501 (2009).

[5] C. C. Margossian, A review of automatic differentiation and its efficient implementation, WIREs Data Mining and Knowledge Discovery **9**, e1305 (2019), _eprint: https://onlinelibrary.wiley.com/doi/pdf/10.1002/widm.1305.

[6] N. Leung, M. Abdelhafez, J. Koch, and D. Schuster, Speedup for quantum optimal control from automatic differentiation based on graphics processing units, Physical Review A **95**, 042318 (2017).

[7] J. Bradbury, R. Frostig, P. Hawkins, M. J. Johnson, C. Leary, D. Maclaurin, G. Necula, A. Paszke, J. VanderPlas, S. Wanderman-Milne, and Q. Zhang, JAX: composable transformations of Python+NumPy programs (2018).

[8] D. P. Kingma and J. Ba, Adam: A Method for Stochastic Optimization (2017), arXiv:1412.6980 [cs].